New Phytologist

Research

Cellular pH measurements in *Emiliania huxleyi* reveal pronounced membrane proton permeability

K. Suffrian[1], K. G. Schulz[2], M. A. Gutowska[1], U. Riebesell[2] and M. Bleich[1]

[1]Physiologisches Institut, CAU Kiel, Olshausenstraße 40, D-24098 Kiel, Germany; [2]Leibniz Institute of Marine Sciences (IFM-GEOMAR), Düsternbrooker Weg 20, D-24105 Kiel, Germany

Author for correspondence:
Markus Bleich
Tel: +49 (0)431 880 2961
Email: m.bleich@physiologie.uni-kiel.de

Received: *13 September 2010*
Accepted: *12 December 2010*

New Phytologist (2011) **190**: 595–608
doi: 10.1111/j.1469-8137.2010.03633.x

Key words: acid–base metabolism, BCECF (2′,7′-bis-(2-carboxyethyl)-5-(and-6)-carboxyfluorescein), bicarbonate transport, dissolved inorganic carbon (DIC), DIDS (4,4′-diisothiocyanatostilbene-2,2′-disulfonic acid), *Emiliania huxleyi,* nigericin, pH homeostasis.

Summary

- To understand the influence of changing surface ocean pH and carbonate chemistry on the coccolithophore *Emiliania huxleyi*, it is necessary to characterize mechanisms involved in pH homeostasis and ion transport.
- Here, we measured effects of changes in seawater carbonate chemistry on the fluorescence emission ratio of BCECF (2′,7′-bis-(2-carboxyethyl)-5-(and-6)-carboxyfluorescein) as a measure of intracellular pH (pH_i). Out of equilibrium solutions were used to differentiate between membrane permeation pathways for H^+, CO_2 and HCO_3^-.
- Changes in fluorescence ratio were calibrated in single cells, resulting in a ratio change of 0.78 per pH_i unit. pH_i acutely followed the pH of seawater (pH_e) in a linear fashion between pH_e values of 6.5 and 9 with a slope of 0.44 per pH_e unit. pH_i was nearly insensitive to changes in seawater CO_2 at constant pH_e and HCO_3^-. An increase in extracellular HCO_3^- resulted in a slight intracellular acidification. In the presence of DIDS (4,4′-diisothiocyanatostilbene-2,2′-disulfonic acid), a broad-spectrum inhibitor of anion exchangers, *E. huxleyi* acidified irreversibly. DIDS slightly reduced the effect of pH_e on pH_i.
- The data for the first time show the occurrence of a proton permeation pathway in *E. huxleyi* plasma membrane. pH_i homeostasis involves a DIDS-sensitive mechanism.

Introduction

Emiliania huxleyi is the most abundant and cosmopolitan calcifying phytoplankton (Paasche, 2002). This coccolithophore with a diameter of 4–5 μm thrives in the euphotic zone of cold temperate to tropical regions (Westbroek *et al.*, 1993). It forms extensive blooms covering up to 250 000 km^2 (Holligan *et al.*, 1983; Balch *et al.*, 2010) and is considered to be responsible for the production of up to 50% of calcite on Earth (Westbroek *et al.*, 1989; Broecker & Clark, 2009). Calcification at the cellular level is related to photosynthesis and acid–base metabolism.

Emiliania huxleyi produces calcite platelets, so-called coccoliths, in a specialized intracellular compartment, the coccolith vesicle (Paasche, 2002), from where they are exocytosed upon completion. For calcification *E. huxleyi* depends on the supply of dissolved inorganic carbon (DIC). The same applies for photosynthesis. As in other algae, primary carbon fixation is CO_2-dependent, as it is mediated by the enzyme Rubisco (ribulose-1,5-bisphosphate carboxylase/oxygenase) in the Calvin–Benson cycle, producing C_3 compounds. However, recent studies have shown a C_4 anaplerotic β-carboxylation reaction, producing C_4 compounds concomitantly operating in *E. huxleyi* (Tsuji *et al.*, 2009). This pathway could supplement the cells as a temporal 'CO_2 storage' in DIC uptake.

Both calcification and photosynthesis have the potential to interfere with cytosolic pH homeostasis. It is therefore of special interest by which mechanisms the cell provides and regulates cell membrane permeability to CO_2, HCO_3^- and H^+.

Membrane permeability for a substrate depends on the lipid composition in addition to the functional expression of membrane proteins such as ion channels, transporters, and pumps. Unfortunately, composition of membrane lipids, membrane proteins, and electrical properties are not well characterized in *E. huxleyi*. CO_2 permeability and a HCO_3^- transport pathway have been suggested (Paasche, 1968, 2002; Nimer *et al.*, 1996; Herfort *et al.*, 2002; Brownlee & Taylor, 2004). Herfort *et al.* (2002) found the HCO_3^- pathway to be sensitive to DIDS (4,4′-diisothiocyanatostilbene-2,2′-disulfonic acid), a relatively unspecific

blocker of a set of anion transporters. In *Coccolithus pelagicus*, a larger coccolithophore, a voltage-dependent and DIDS-inhibitable Cl^- current was shown (Taylor & Brownlee, 2003).

More information is available on pH_i in coccolithophores. Presently there are three datasets on pH measurements in *E. huxleyi*, reporting a whole-cell pH of between 6.77 ± 0.31 for a low calcifying strain and 7.29 ± 0.11 for a high calcifying strain (Dixon *et al.*, 1989; Nimer *et al.*, 1994a). Cytosol pH was reported to be *c.* 7.0 (Dixon *et al.*, 1989; Anning *et al.*, 1996), pH of the chloroplast 8.0 (Anning *et al.*, 1996), and pH inside the coccolith vesicle was measured to be 7.1 ± 0.3 (Anning *et al.*, 1996). At a seawater pH of *c.* 8.1, the H^+ gradient across the plasma membrane is about one order of magnitude (Dixon *et al.*, 1989; Anning *et al.*, 1996). This might reflect either high cytosolic H^+ production at a limited export capacity, or H^+ uptake mechanisms driven by ion gradients or membrane voltage, or both processes at the same time.

In the present study we monitored BCECF (2′,7′-bis-(2-carboxyethyl)-5-(and-6)-carboxyfluorescein) fluorescence in *E. huxleyi* as a measure of cytosolic pH. The use of the pH-sensitive dye BCECF is a well-established method to measure pH_i in different organisms since the early 1980s (Rink *et al.*, 1982). It is introduced into the cells as an uncharged acetoxymethyl ester form (BCECF-AM), and only emits fluorescence, after cleavage to the free acid by (cellular) esterases. This hydrolysis also traps the dye inside the cells, as the BCECF molecule is now charged (see also Pörtner *et al.*, 2010). The BCECF signal can be calibrated after permeabilization of the plasma membrane by the H^+/K^+ exchanger nigericin and elimination of the transmembrane K^+ gradient. Calibration has to be performed at the end of every single experiment to obtain individual pH_i values, whereas ratio changes as a measure of pH_i are fairly constant between experiments.

With this method we got a first semiquantitative insight into the membrane permeability properties with respect to CO_2, HCO_3^-, and H^+. The challenge in these experiments was to differentiate between isolated effects of CO_2, HCO_3^-, and H^+ on physiological processes. Under steady-state conditions it is impossible to alter one of the three carbon species while keeping the other two constant because they are in a dynamic equilibrium (Eqn 1).

$$CO_2 + H_2O \rightleftarrows HCO_3^- + H^+ \rightleftarrows CO_3^{2-} + 2H^+ \quad \text{Eqn 1}$$

Different approaches have been applied to overcome this problem, taking advantage of the slow reaction rates between CO_2 and HCO_3^-. The isotopic disequilibrium technique (Rost *et al.*, 2002; Endeward *et al.*, 2006) combines radioactive or stable isotopes of the CO_2 and HCO_3^- pools with mass spectrometric measurements of the resulting metabolites. The out-of-equilibrium (OOE) approach (Zhao *et al.*, 1995) allows the impact of any of the three species on pH_i to be monitored online and at a single cell level.

We used the OOE method to investigate membrane permeability properties for H^+, CO_2 and HCO_3^- and used DIDS as a pharmacological tool.

Materials and Methods

Cell culture

Emiliania huxleyi cells used in this study were isolated in 2005 during the PeECE III mesocosm study in the Raune Fjord (Norway) by M. N. Müller (Riebesell *et al.*, 2007). The cultures were grown in artificial seawater (ASW) modified from Kester *et al.*(1967), with an initial pH of 8.05 ± 0.05 (Table 1) and enriched with nutrients according to f/20-Si, modified after Guillard (1975). Cells were exposed to daylight (Osram Lumilux L 18W/950 Color Proof Daylight G13; Osram, Munich, Germany) in a simulated diurnal cycle with a maximum photosynthetically active radiation (PAR, 400–700 nm; QSL-2101, Biospherical Instruments, San Diego, CA, USA) of 170 μmol photons m^{-2} s^{-1} for 6 h, framed by a 6 h increment and a 6 h decrement in three steps, respectively. The mean PAR during the illumination phase was 100 μmol photons m^{-2} s^{-1}. Cells were kept at 17°C in a growth chamber (KBWF 240, Binder GmbH, Tuttlingen, Germany) in 50 ml polystyrene culture flasks (Sarstedt, Nümbrecht, Germany).

For the experiments, cells were grown to high densities (4×10^5–1.8×10^6 cells ml^{-1}, achieved during days 7–10) under nutrient limitation (from day 3–4 onwards) to get a highly calcified cell population (Shiraiwa, 2003), which was found to be best suitable for the experiments as a result of high cell numbers, good loading properties and increased adhesiveness to the bath chamber.

Decalcification and protoplast isolation

A quantity of 10–15 ml of cell culture was centrifuged at 1882 ***g*** for 5 min and the supernatant was discarded. The cell pellet was resuspended in an ethylene glycol-bis(2-aminoethylether)-*N,N,N′,N′*-tetraacetic acid-containing solution (EGTA, solution 3, ASW_{strip}) by gentle mixing with a plastic transfer pipette and then incubated for 15 min to detach and dissolve the coccoliths (adapted from Taylor & Brownlee, 2003). Cells were centrifuged again and incubated in ASW_{strip} for another 10 min. Thereafter, cells were mechanically agitated by a series of rapid aspirations and expulsions through polyethylene tubing (inner diameter 350 μm) attached to a 1 ml syringe to remove remnants of coccospheres. After another centrifugation step, the cells were transferred to solution 2 (ASW_c, pH 8.05 ± 0.05) where they were kept for 2 h to allow recovery. Apart from

Table 1 Artificial seawater (ASW) solutions (data are mmol kg^{-1})

		1	2	3	4	5
	Seawater	$ASW_{culture}$	ASW_c	ASW_{strip}	0 HCO_3^-	ASW_{nig}
Na^+	498	504	504	447	488	437
K^+	9.9	9.9	9.9	10.0	10.0	97.4
Mg^{2+}	53	53	53	50	53	52
Ca^{2+}	10.4	10.3	10.3	0	10.0	9.7
Sr2+	0.09	0.09	0	0	0	0
Cl^-	546	544	545	555	569	532
SO_4^{2-}	28	28	28	0	28	27
Br^-	0.84	0.82	0	0	0	0
F^-	0.07	0.07	0	0	0	0
H_3BO_3	0.42	0.42	0	0	0	0
HCO_3^-	1.98	2.35	2.35	2.00	0	0
HEPES	0	0	0	0	5	5
Gluconate	0	37.6	37.6	0	0	71
EGTA	0	0	0	25	0	0
Calculated values (CO2SYS)						
HCO_3^-		2.14		1.80		
CO_3^{2-}		0.19		0.19		
CO_2		0.02		0.01		
pCO_2 [μatm]		592.40		363.20		
pH		8.08 ± 0.03			*(as ind.)*	*(as ind.)*
Osmolality		1070 ± 10				
Salinity		35 ± 1				

ASW_c, control ASW; $ASW_{culture}$, ASW used for culture; ASW_{nig}, calibration solution containing 100 mmol kg^{-1} K^+ and 10 μmol kg^{-1} nigericin; ASW_{strip}, EGTA-containing solution; as ind., as indicated in the respective results.
ASW solutions were designed according to values of pH, osmolality and salinity measured in North Sea water. Standard seawater composition was modified after Zeebe & Wolf-Gladrow (2001). All solutions were allowed to equilibrate and, if necessary, adjusted to the exact pH at 20°C (NaOH or HCl). ±, indicator of the accuracy achieved and allowed in generation of the respective solution.

centrifugation, all steps were performed under illumination to allow photosynthesis during the long stripping process.

Dye loading (BCECF)

Stock solutions of BCECF-AM (10 mmol l^{-1} in dimethyl sulfoxide, Invitrogen), and Pluronic F-127 (10% in H_2O, Invitrogen) were stored in aliquots at −20°C until use. Cells were incubated at 17°C with a final concentration of 50 μmol l^{-1} BCECF-AM and 0.5% Pluronic for 120 min in ASW to allow sufficient uptake and cleaving of the esterified dye. Cells were centrifuged and the supernatant was discarded. After resuspension in ASW, cells were transferred into the bath chamber and allowed to settle and adhere to the poly-D-lysine-coated bottom cover slip (Sigma-Aldrich) for at least 30 min. Thereafter a sufficient number of cells firmly adhered and allowed a rapidly flowing bath solution. With this dye loading procedure we achieved a signal-to-noise relation for the emission signal > 10 throughout a 1 h experimental period in most cells. Cells with weak dye loading below this threshold or showing signs of overloading were excluded.

Viability tests

To ensure that the cells were viable after the isolation and incubation procedure, we added trypan blue (458 μmol l^{-1}) to test samples and monitored dye uptake. Exclusion of the dye was expected for intact protoplasts and observed in > 90% of the tested cells. In a second approach we tested the ability of cell samples to recalcify under normal cell culture conditions. Virtually all of the observed cells were able to recalcify within the observation period of 2 d and the culture did not show any significant change in growth rate compared with the control.

Microfluorimetry

Fluorescence was monitored with an imaging system (Visitron) using a charge coupled device (CCD) camera (CoolSNAP HQ^2; Photometrics, Tucson, AZ, USA) mounted on an inverted microscope (Zeiss Axiovert 35 M). The microscope was equipped with an A-Plan 100×/1.25 Oil objective (×100, Zeiss, Jena, Germany). At a rate of 0.2 Hz the dye was alternatively excited at 486 and 440 nm (± 10 nm bandwidth) for 24 and 60 ms, respectively. Emission was recorded at 525 nm (emission filter ET525/50 nm; Chroma Technology Corp, Bellows Falls, VT, USA) and the integrated ratio of the emission intensities at the two excitation wavelengths over the whole cell was calculated after subtraction of system immanent camera offset and background signal (MetaFluor Meta Series Software 7.6.1; Meta Imaging System, Molecular Devices, Inc., Sunnyvale, CA, USA). From each experiment five to 20 cells were selected for analysis, and each cell was analysed individually for fluorescence ratio, representing pH_i. Our study focussed on changes in pH_i as a result of changes in ambient CO_2, HCO_3^- and H^+ concentrations and we decided not to perform an individual calibration for each cell. However, in order to gain a magnitude for pH_i changes we performed a calibration of the ratio change in a separate experimental series.

The cells were checked for autofluorescence after excitation at the experimental wavelengths 486 and 440 nm, known to induce chlorophyll autofluorescence. No autofluorescence was detected at the emission wavelength of 525 ± 25 nm.

Calibration of ΔpH_i with nigericin

Nigericin was used (Pressman, 1976) to calibrate relative changes in pH_i of living cells. It is an ionophore and acts as a K^+/H^+ exchanger. To obtain absolute pH_i measurements, $[K^+]_e$ in calibration solutions has to be adjusted to equal

$[K^+]_i$ in order to remove the driving force for K^+ and to depolarize the cell. Under these conditions, internal and external $[H^+]$ can equilibrate. Values for $[K^+]_i$ in *E. huxleyi* have been reported over a wide range from 100 to 260 mmol l^{-1} (Sikes & Wilbur, 1982; Ho *et al.*, 2003). Hence, we limited our calibration to relative changes in pH_i as this only requires high $[K^+]_e$.We did not calculate absolute pH_i values in this study.

A stock solution of nigericin (Nigericin sodium salt, 72445, Sigma Aldrich, 10 mmol l^{-1} in ethanol) was prepared and stored in aliquots at −20°C until use.

Emiliania huxleyi cells were exposed to 10 μmol l^{-1} nigericin in the presence of 100 mmol l^{-1} K^+ (solution 5) at varying pH values. Ratio changes were monitored (Fig. 4a,b). The calibration curve (Fig. 4c) was linear, allowing an estimate to be made of the relationship between the detected change in emission ratio of BCECF and the respective change in pH_i.

Experimental procedure

General For all experiments the bath chamber (350 μl volume) was mounted on the stage of an inverted microscope and perfused by gravity at a rate of 6–8 ml min^{-1} at 17°C, ensuring rapid bath exchange rates. In this background of bath perfusion, OOE solutions were directly applied to the investigated cells by a micromanipulated superfusion pipette system, enabling the mixing time to be kept < 10 s. During application of the OOE solutions, the bath was continuously rinsed by solution 2 (ASW_c), securing permanent removal of the OOE solution.

The sequence of bath solution exchanges is described in detail for each series in the respective Results section.

OOE mixing unit Dual-syringe pumps (50 ml, Perfusor Secura, B. Braun, Messungen, Germany) were used to drive solution pairs a and b (Table 2) at a constant rate of 7–10 ml h^{-1} to a Teflon mixing unit (Supporting Information, Fig. S1) with six inlets, each secured with a unidirectional restrictor valve, for a consecutive application of up to three OOE solutions. Stainless steel inlet pairs for the 1 : 1 combination of a and b solutions were situated opposite to ensure optimal mixing. In addition, mixing was improved and dead space minimized by a mesh (60 μm pore size nylon filter, Millipore NY60) mounted inside the mixing unit in front of the outflow cannula. The opening of this cannula was positioned directly before and above the cells (*c.* 30° lateral) under investigation to ensure laminar superfusion and to prevent any mixing of solutions around the cells. The total dead space volume of the system after mixing was *c.* 20 μl. In consequence, the time between mixing and supply of OOE solutions to the cells was 7–10 s, and thus well within the time required to prevent any significant equilibration (see Fig. 1).

Table 2 Out-of-equilibrium (OOE) solutions (data are mmol kg^{-1})

	6a	6b	6	7a	7b	7
	High CO_2		(a + b) OOE	High HCO_3^-		(a + b) OOE
Na^+	484	415	450	563	361	462
K^+	10	10	10	10	10	10
Mg^{2+}	52	52	52	0	103	52
Ca^{2+}	10	10	10	0	19	10
Cl^-	563	494	528	530	508	519
SO_4^{2-}	27	27	27	0	55	27
HEPES	0	63	31.7	0	63	31.7
HCO_3^-	0	0	0	43	0	21
CO_2 (%)	5	0	2.4	0	0	0
Calculated values						
HCO_3^-	0.1	0	0.05	10.6	0	20
CO_3^{2-}	0	0	0	33.4	0	2
CO_2	1.72	0	0.86	0	0	0
(%)	5.0	0	2.5	0	0	0
pH	4.90	8.07	8.08	9.24	7.69	8.07
Osmolality			1070 ± 10			
Salinity			35 ± 1			

OOE solutions a and b were adjusted or aerated to the measured pH value at 20°C. Solutions were generated shortly before application in the experiment. ±, indicator of the accuracy achieved and allowed in generation of the respective solution.

pH measurements in experimental solutions pH was measured with a pH-sensitive single-rod measuring cell (Blueline 16 pH; Schott Instruments, Mainz, Germany) with a microprobe. This enabled us to measure the pH of seawater (pH_e) directly at the outlet of the OOE mixing unit to check for target pH. pH values are presented on the NBS (National Bureau of Standards, USA) scale and a pH of 8.05 ± 0.05 was defined as the control pH. Values in Fig. 1, however, are given on free scale.

Solutions

ASW solutions Artificial seawater solutions were designed after Zeebe & Wolf-Gladrow (2001). At a sea surface temperature of 17°C, a pH of 8.2 on the NBS scale and a salinity of 35, the carbonate system consists of 1900–2000 μmol kg^{-1} HCO_3^-, 200 μmol kg^{-1} CO_3^- and 15 μmol kg^{-1} CO_2. Osmolality and salinity (35 ± 1) were chosen according to measurements of natural seawater (NSW). All experimental solutions (Table 1) were adjusted to an osmolality of 1070 ± 10 mosm kg^{-1} at the expense of NaCl or by addition of Na-gluconate. pH, if not indicated otherwise, was 8.08 ± 0.05. Calculations for the carbonate system were performed using CO2SYS (Lewis & Wallace, 1998), based on measurements of pH and total inorganic carbon concentration. Dissociation constants (K_1, K_2) for carbonic acid were taken from Roy *et al.* (1993), KSO_4^- from Dickson (1990). pH was measured and calculations are given on the NBS scale. All chemicals were purchased at highest grade of purity

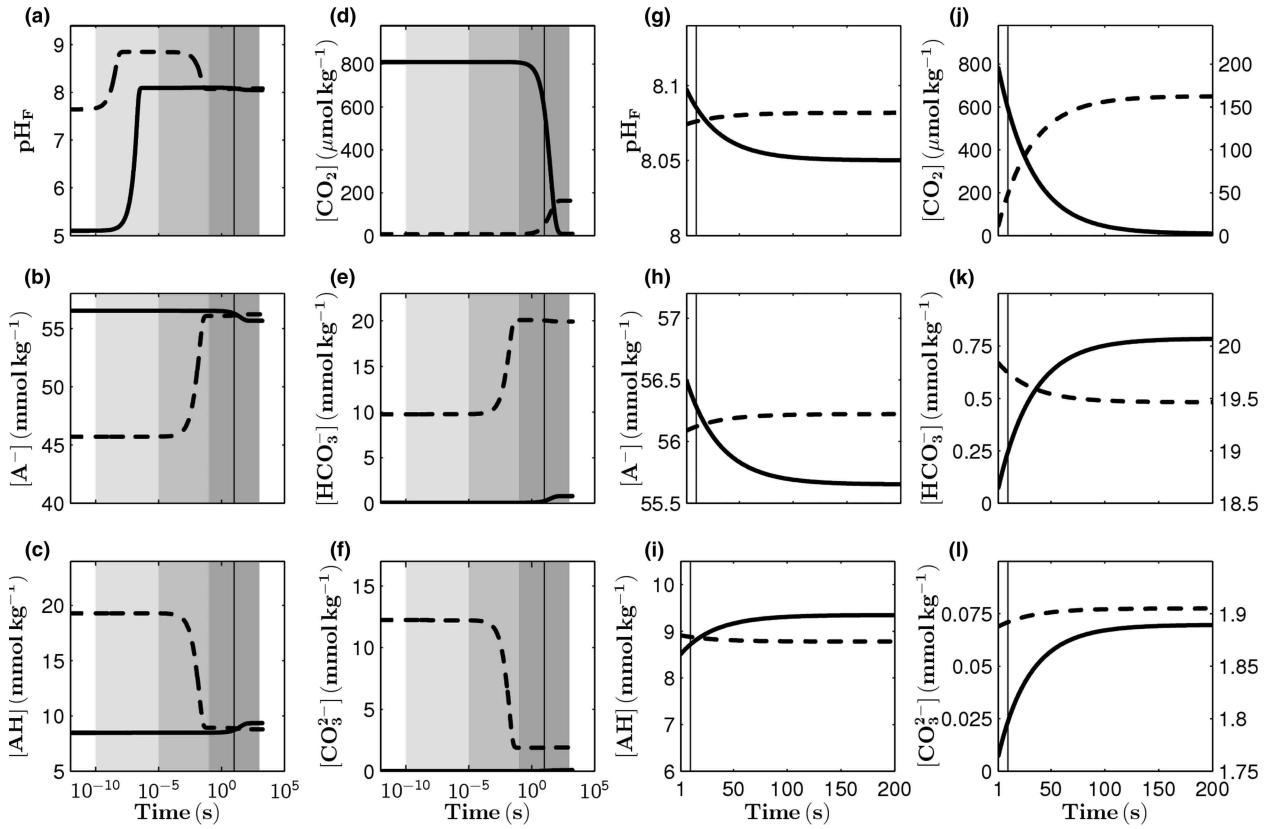

Fig. 1 Reaction kinetics upon mixing of out-of-equilibrium (OOE) solutions. Changes in concentrations against time upon mixing of two solutions (see Table 2) with different carbonate chemistry on a logarithmic scale (10^{-10}–10^5 s) (a–f) and on a linear scale (1–200 s) (g–l). Shown are pH on the free scale, pH_F (a, g); concentrations of the unprotonated form of HEPES, [A^-] (b, h); the protonated form of HEPES, [AH] (c, i); carbon dioxide [CO_2] (d, j); bicarbonate, [HCO_3^-] (e, k); carbonate, [CO_3^{2-}] (f, l). Solid lines illustrate evolution of carbonate chemistry speciation in solution 6 (high CO_2). Dashed lines show carbonate chemistry kinetics in solution 7 (high HCO_3^-). Calculations of carbonate chemistry speciation were done at a salinity of 35 and at 20°C. The vertical line represents the experimental time range of 7–10 s after mixing. Light, intermediate and dark gray shaded areas mark the time ranging from 10^{-10} to 10^{-5}, 10^{-5} to 10^{-1} and 10^{-1} to 1000 s, respectively. Note that the left ordinates in (j–l) give the values for the solid lines (high CO_2), while the additional right ordinate in (j–l) gives the values for the dashed lines (high HCO_3^-).

from Merck and Sigma, Germany. DIDS was dissolved in dimethyl sulfoxide (DMSO) at a stock concentration of 0.1 mol l^{-1} and added at a final concentration of 0.1 mmol l^{-1} to the respective experimental solutions, unless indicated otherwise. DMSO did not exceed a concentration of 0.1%. DIDS autofluorescence did not interfere with BCECF fluorescence at the selected wavelengths.

OOE solutions Out-of-equilibrium solutions were designed to have either a comparatively high [CO_2] and low [HCO_3^-], or a high [HCO_3^-] and a very low [CO_2], at a typical surface ocean pH of 8.05. The enzymatically catalyzed equilibration of experimental solutions directly at the extracellular surface of the cells was neglected since, in *E. huxleyi*, only very low external carbonic anhydrase (CA) activities have been observed under various conditions (Rost *et al.*, 2003, 2006). Although there is strain variance and there might be strains with higher CA expression and activity, dependent on nutrient concentration (Nimer *et al.*, 1994b), no CA inhibitors were added as they might have dampened cytosolic reactions in pH homeostasis.

A chemical model of the carbonate system, including all important reactions in seawater together with HEPES buffer kinetics, was implemented according to Schulz *et al.* (2006). The resulting seven differential equations were integrated numerically with the matlab 'ode15s' solver for 'stiff' problems (Shampine & Reichelt, 1997), and used to calculate the reaction kinetics in carbonate chemistry speciation upon mixing of two different OOE solutions. The model also allows the degree of disequilibrium at any given point in time to be estimated and the actual concentrations of, for instance, [H^+], [CO_2] and [HCO_3^-] to be derived.

Calculations and statistics

Each cell was analyzed individually for changes in emission ratio as a measure of pH_i and the resulting changes are shown as means ± SEM. Data were pooled from multiple

cells in different experiments where (n, m) indicate the number of cells (n) from m experiments. Paired Student's t-test was applied, and $P < 0.01$ was accepted for statistical significance. Statistics and calculations were performed using Excel 2003 (Microsoft) or OriginPro 7.5G (OriginLab Corporation, Northampton, MA, USA). Absolute and relative changes were calculated vs values derived under control conditions unless indicated otherwise.

Results

OOE solutions

The present experiments with OOE solutions were performed in the time range 7–10 s after mixing of the respective solution pairs a and b. We calculated the reaction kinetics for the carbonate chemistry according to Schulz *et al.* (2006). The results nicely validate the fact that the cells under investigation were exposed to solutions that were still out of equilibrium (Fig. 1). We generated two OOE solutions with either high $[CO_2]$ or high $[HCO_3^-]$. The two solutions are depicted as a solid line (high $[CO_2]$) and a dashed line (high $[HCO_3^-]$). The development of the solutions can be identified in Fig. 1(d) and (e), which show $[CO_2]$ and $[HCO_3^-]$ vs time. The time axis is logarithmic and covers the whole period from initial mixing to equilibrium. The time range of the experiment is indicated by a vertical line.

The high-CO_2 solution (solid line) shows a virtually constant $[CO_2]$ until *c.* 1 s (Fig. 1d) and remains above *c.* 600 μmol kg^{-1} CO_2 during the 7–10 s experimental period. The formation of HCO_3^- during this period is negligible (Fig. 1e). Only after minutes does the conversion of CO_2 into HCO_3^- reach equilibrium. The target pH value in this solution is already met 10 μs after mixing (Fig. 1a).

The high-HCO_3^- solution (dashed line) shows a substantial increase in $[HCO_3^-]$ to the target value in the time range of ms (Fig. 1e) by the protonation of CO_3^{2-} (Fig. 1f). This value stays virtually constant during the time of the experiment. CO_2 formation in this solution does not exceed 50 μmol kg^{-1}. In this solution the target pH value is reached within ms after mixing (Fig. 1a). The initial pH changes reflect buffering and protonation of CO_3^{2-}.

Fig. 1(b) and (c) show the respective changes in HEPES buffer components. For a higher time and concentration resolution of the equilibration phase refer to Fig. 1(g)–(l), plotted with linear time axis. The left ordinate gives the scale for the high-CO_2 solution (solid line), the right ordinate for the high-HCO_3^- solution (dashed line). In essence, the slow conversion between CO_2 and HCO_3^- allows the use of OOE solutions in the time-frame between 0.1 and 10 s after mixing without relevant equilibration. Even after 10 s the most obvious change in $[CO_2]$ in the high-CO_2 solution (Fig. 1j) results in a $[CO_2]$ that is still threefold above $[HCO_3^-]$ in the same solution.

BCECF measurements

After dye loading, *E. huxleyi* was allowed to equilibrate for a few minutes to control conditions, resulting in a stable ratio after initial rundown. Experiments were started *c.* 120 s thereafter. The resulting BCECF fluorescence ratio as a measure of pH_i resembled a Gaussian distribution over all analysed experiments (Fig. 2a). This was also observed for batches of cells within one experiment, indicating different individual starting pH_i values. Since our study focussed on the changes of pH_i as a result of changes in ambient CO_2, HCO_3^- and H^+ concentrations, we decided not to perform an individual calibration for each cell and therefore we do not give absolute pH_i values. The mean ratios under control conditions in the experimental series (Table 3) were between 2.49 and 2.54. In some experiments we observed a decline in ratio over time. Cells with a lower loading signal were monitored in the same experiments, and showed qualitatively the same results (data not shown); however, because of the low signal, the effect was dampened and the signal approached the detection limit already before completion of the experiment.

Confocal imaging of *E. huxleyi* showed an intracellular dye distribution of the entire cell excluding the chloroplast (Fig. 2b; also see discussion on dye loading and pH_i).

Effect of H^+

In a first series of experiments we investigated the effect of acidic seawater on pH_i. Fig. 3(a) shows an original experiment where solution 2 (ASW_c) was rapidly changed from pH_e 8 to pH_e 6. pH_i of *E. huxleyi* declined instantaneously with bath exchange. The kinetics of acidification was almost as fast as the bath exchange rate, which was rapid. We did not observe any compensation of pH_i during exposure to acidified conditions. When the acidified ASW was again exchanged for ASW_c, pH_i increased again; however, in some cells the effect was not completely reversible.

To differentiate between CO_2 and H^+ effects on pH_i, we repeated these experiments in the absence of HCO_3^- and CO_2 (solution 4). Again we observed the same pattern of cytosolic acidification (Fig. 3b, Table 3a): pH_i decreased instantaneously responding to pH_e and reached a new stable pH_i. At a pH_e of 7.0 we observed a mean decrease in the ratio of 0.56 ± 0.04, corresponding to a relative decrease of 22 ± 1.3% (n = 42, m = 3). Even if the length of the exposure to the increased $[H^+]$ was extended, we did not observe any cellular compensation mechanism to re-establish the initial pH_i while under acidified conditions. Only upon return to control conditions was the pH_i effect reversible.

A concentration–response curve for the dependence of pH_i on pH_e is shown in Fig. 3(c). The relationship (Fig. 3d) was linear over the physiological range between pH_e values of 6.5 and 9.0 (R^2 = 0.96, n = 31, m = 6; Table 3b).

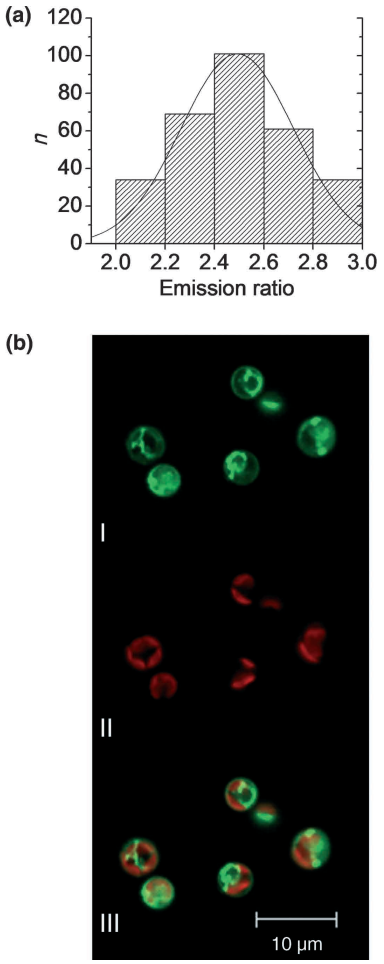

Fig. 2 Frequency distribution of measured emission ratios of BCECF (2′,7′-bis-(2-carboxyethyl)-5-(and-6)-carboxyfluorescein) fluorescence and confocal images showing dye distribution. (a) Analysis of the distribution of measured emission ratios under initial control conditions of n = 299 cells displayed as absolute number in clusters of 0.2. (b) Confocal false color image of *Emiliania huxleyi* cells loaded with BCECF-acetoxymethyl ester (BCECF-AM). (I) BCECF fluorescence intensity, green (excitation 488nm, bandpass 530–550 nm). (II) Chloroplast autofluorescence intensity, red (excitation 488 nm, emission long pass 600 nm). (III) Merged image indicates differential localization of fluorescence signals. No BCECF loading of chloroplast.

Calibration of ΔpH_i with nigericin

In a separate series of experiments we calibrated the changes in ratio for pH_i changes with the nigericin method (Fig. 4a,b). A direct comparison of the effect of extracellular acidification in the absence and presence of nigericin on fluorescence ratio shows that the change in ratio induced by a pH_e change is greater and faster in the presence of nigericin. This demonstrates the additional H^+ permeability introduced into the plasma membrane by nigericin at high $[K^+]$. The calibration curve was linear in the investigated pH range between 6.5 and 8.5. Changes in 0.78 fluorescence ratio units corresponded to a change of one unit in pH_i (Fig. 4c).

In the H^+ permeability experiments the slope was shallower. A change of 1 pH_i unit corresponded to a ratio change of 0.44 (Fig. 3d).

In a further series of experiments using OOE solutions we tested the effects of isolated changes in $[CO_2]$ and $[HCO_3^-]$ on pH_i.

High CO_2

To challenge the cell with a high $[CO_2]$ and to monitor the respective changes in pH_i, we exchanged solution 2 (ASW_c, pH 8.05 ± 0.05) for solution 6 (pH 8.08, > 600 µmol CO_2 kg^{-1}, 0.25 mmol kg^{-1} HCO_3^-). No significant effect on pH_i could be detected (−0.01 ± 0.01, P = 0.18, n = 148, m = 8; Fig. 5, Table 3a) in the time range of up to 3 min exposure to high CO_2.

High HCO_3^-

In the same manner we challenged the cells by high extracellular $[HCO_3^-]$. Control solution 2 (ASW_c, pH 8.05 ± 0.05) was exchanged for solution 7 (pH 8.07, *c.* 20 mmol kg^{-1} HCO_3^-, *c.* 50 µmol kg^{-1} CO_2) and the pH_i of *E. huxleyi* cells was monitored again. Interestingly, the ratio as a measure of pH_i decreased significantly by 0.12 ± 0.01 units, which corresponds to a relative decrease of 5 ± 0.3% (P < 0.01, n = 85, m = 5; Fig. 5, Table 3a). The effect of HCO_3^- was reversible upon return to control.

The isolated effects of CO_2, HCO_3^- and H^+ are summarized in Fig. 5(b).

Effect of DIDS

4,4′-Diisothiocyanatostilbene-2,2′-disulfonic acid has been shown to interfere with a variety of membrane proteins involved in pH homeostasis in different species. To investigate whether there is a DIDS-inhibitable transport system expressed and functionally relevant in *E. huxleyi*, we measured the effect of DIDS on pH_i. Application of DIDS in solution 2 (ASW_c) acidified the cell (Fig. 6a). This effect on pH_i was concentration-dependent (Fig 6b; n = 11, m = 2). The effect of DIDS, however, was irreversible.

In a second series of experiments we tested whether the acidification by DIDS was dependent on external HCO_3^-. As shown in Fig. 6(c) and (d) DIDS (100 µmol l^{-1}) still decreased pH_i, indicating that this effect did not depend on external HCO_3^- (n = 46, m = 3).

Finally we investigated whether DIDS influenced the effect of pH_e on pH_i. In the absence of HCO_3^- we compared the effect of pH_e 7 on pH_i in the presence and absence of DIDS (100 µmol l^{-1}). As shown in Fig. 6(e) the effect of pH_e 7 was slightly reduced in the presence of DIDS. A

Table 3 Effects of changes in CO_2, HCO_3^- and H^+ on intracellular pH (pH_i)

Solution		(mol kg^{-1})	*n*	*m*	Mean	d_{abs}	*d* (%)	*P*
(*a*)								
7	HCO_3^-	0.0220	85	5	2.31 ± 0.02	−0.12 ± 0.01	−5 ± 0.3	< 0.01
6	CO_2	0.0017	148	8	2.42 ± 0.02	−0.01 ± 0.01	−1 ± 0.4	0.18
4	H^+	1×10^{-7}	42	3	1.93 ± 0.03	−0.62 ± 0.04	−24 ± 1.3	< 0.01
4	H^+_{DIDS}	1×10^{-7}	46	3	1.70 ± 0.04	−0.40 ± 0.02	−19 ± 1.0	< 0.01
Solution	pH_e	H^+ (mol kg^{-1})	*n*	*m*	Mean	d_{abs}	*d* (%)	*P*
(*b*)								
4	9.0	1×10^{-9}	31	6	2.62 ± 0.05	−0.13 ± 0.02	−5 ± 0.7	< 0.01
	8.5	5×10^{-9}			2.49 ± 0.05	−0.18 ± 0.03	−7 ± 1.3	< 0.01
	8.0	1×10^{-8}			2.31 ± 0.04	−0.28 ± 0.02	−7 ± 1.3	< 0.01
	7.5	5×10^{-8}			2.03 ± 0.03	−0.27 ± 0.02	−12 ± 0.9	< 0.01
	7.0	1×10^{-7}			1.77 ± 0.04	−0.20 ± 0.02	−11 ± 1.0	< 0.01
	6.5	5×10^{-7}			1.57 ± 0.04			

Control solution 2 (ASW_c) was exchanged by the respective experimental solution. Mean values give fluorescence ratio as a measure of pH_i. (a) Effects of HCO_3^-, CO_2, H^+ and H^+ in the presence of 4,4′-diisothiocyanatostilbene-2,2′-disulfonic acid (DIDS, 0.1 mmol l^{-1}). Changes by CO_2 and HCO_3^- were compared with the mean of pre-control and washout. Changes by H^+ were compared with pre-control with and without DIDS, respectively. $P < 0.01$ indicates significant difference vs the respective control value. Relative changes in ratio differed significantly ($P < 0.01$). (b) Concentration response of pH_i to changes in pH_e. Ratio changes were calculated relative to the previous pH_e step. *n*, number of individual cells; *m*, number of experiments; Mean, average ratio; d_{abs}, absolute change in ratio; *d* (%), relative change; $P < 0.01$ indicates significant difference vs the respective previous pH step; pH_e, pH of seawater.

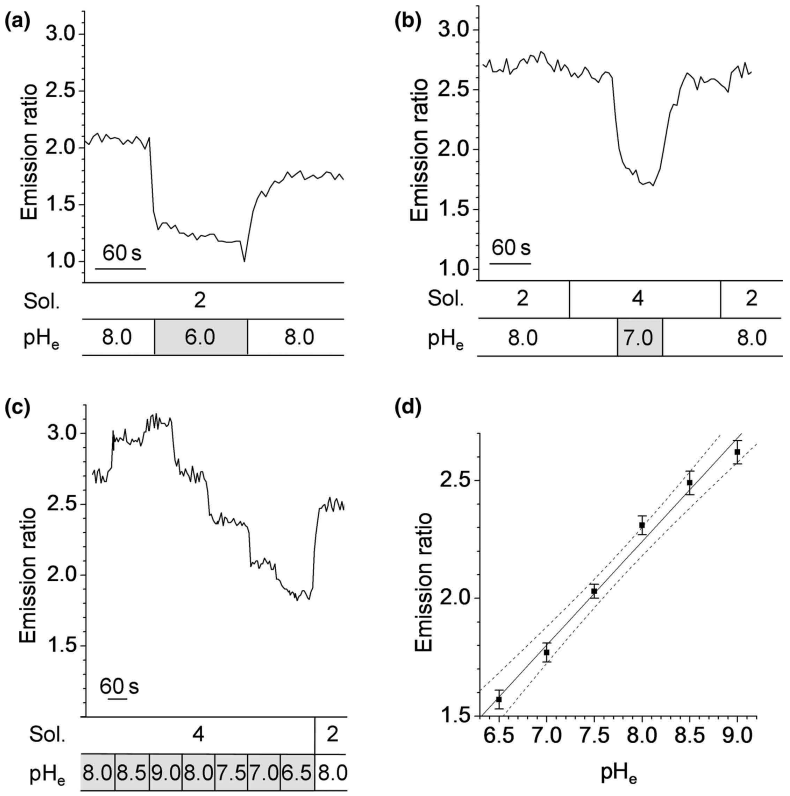

Fig. 3 Effect of $[H^+]$ on intracellular pH (pH_i). Original recordings of fluorescence ratio as a measure of pH_i in representative single cells of *Emiliania huxleyi*. (a) Effect of change in pH of seawater (pH_e) from 8 to 6 in control artificial seawater (ASW_c, solution (Sol.) 2). (b) Effect of change in pH_e from 8 to 7 in the absence of HCO_3^- (Sol. 4). (c) Concentration response in a representative single cell. (d) Summary of 31 cells ($m = 6$). pH_i followed pH_e in a linear relationship over the physiological range ($\Delta ratio/\Delta pH_e = 0.44$; $R^2 = 0.96$). Dotted line, 95% confidence interval.

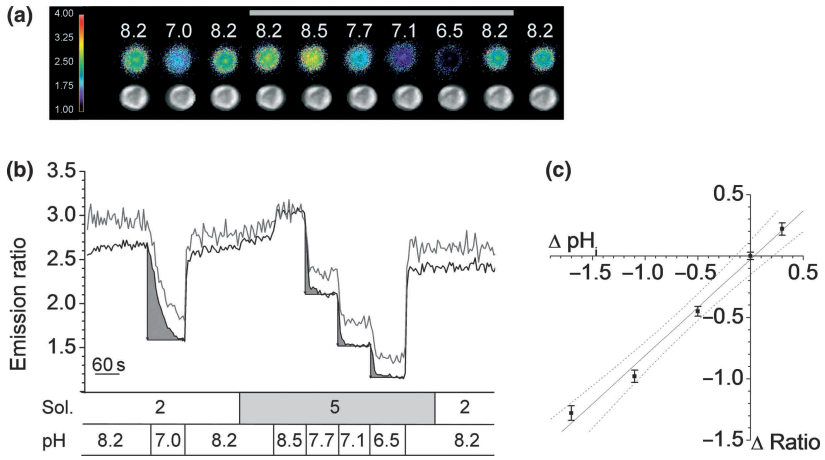

Fig. 4 Calibration of ΔpH_i (intracellular pH) with nigericin. Original recordings of fluorescence ratio as a measure of pH_i in representative single cells of *Emiliania huxleyi*. (a) Time series (left to right, upper row) of ratio images (false color), showing the effect of changes in pH of seawater (pH_e) on BCECF (2′,7′-bis-(2-carboxyethyl)-5-(and-6)-carboxyfluorescein) fluorescence ratio in one cell. The background was subtracted before analysis, and only signal from the cellular region was analyzed. The gray bar indicates the presence of nigericin. In the lower row, the respective intensity images are shown for the same cell, indicating sufficient dye signal throughout the calibration procedure. (b) Concentration response in two representative single cells (black line: cell shown in a). The effect on the ratio as a measure of pH_i by a change in pH_e is shown vs changes in pH_i in the presence of nigericin (solution (Sol.) 5). Dark gray areas under the ratio curve show differences in kinetics without (left) and with (right) nigericin. (c) Calibration curve for pH_i changes: $\Delta ratio/\Delta pH_i = 0.78$; $R^2 = 0.99$, $n = 11$, $m = 6$. Dotted line, 95% confidence interval. Sol. 2, control artificial seawater.

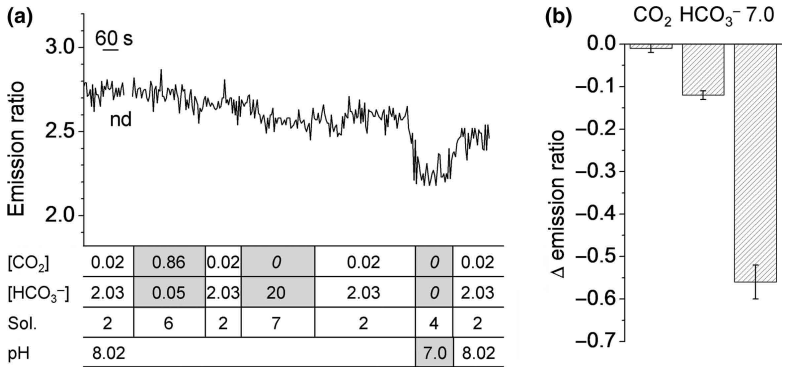

Fig. 5 Effect of high $[CO_2]$ and high $[HCO_3^-]$ out of equilibrium (OOE) on intracellular pH (pH_i). pH_i response on high $[CO_2]$ and high $[HCO_3^-]$ under OOE conditions in comparison to the effect of low pH_e. (a) Original recording of fluorescence ratio as a measure of pH_i in a representative single cell of *Emiliania huxleyi*. (b) Absolute change in ratio (Δ). CO_2, $n = 148$, $m = 8$, $P = 0.15$; HCO_3^-, $n = 54$, $m = 5$, $P < 0.01$; pH 7, solution (Sol.) 4, $n = 42$, $m = 3$, $P < 0.01$; Sol. 2, control artificial seawater; Sol. 6, High $[CO_2]$ OOE solution; Sol. 7, High $[HCO_3^-]$ OOE solution. (nd, data points not determined in this experiment.)

change from pH_e 8 to 7 caused a decrease in fluorescence ratio by 0.62 ± 0.04 ($n = 46$, $m = 3$) under control conditions and by 0.34 ± 0.02 ($n = 46$, $m = 3$, Table 3a) in the presence of DIDS, corresponding to relative changes of 24 ± 1.3% and 19 ± 1.0%, respectively ($P < 0.01$).

Discussion

In this study we present changes in fluorescence ratio as a measure of changes in pH_i. These changes were comparable and consistent between different experiments and cells. For the first time we show that the *E. huxleyi* plasma membrane is highly permeable to H^+.

OOE solutions

$[CO_2]$, $[HCO_3^-]$, $[CO_3^{2-}]$ and $[H^+]$ in seawater are in equilibrium with each other. Typical concentrations in the surface ocean are *c.* 15 μmol kg^{-1} CO_2, *c.* 2000 μmol kg^{-1} HCO_3^- and *c.* 200 μmol kg^{-1} CO_3^{2-} at a pH of *c.* 8.1. This equilibrium is currently shifting to higher $[CO_2]$ and thus higher $[H^+]$ as a result of oceanic uptake of anthropogenic CO_2. Natural changes in surface ocean carbonate chemistry are driven by air/sea gas exchange and biological processes, such as photosynthesis, respiration and calcification. To better understand the observed responses of *E. huxleyi* to changes in seawater carbonate chemistry, it is important to

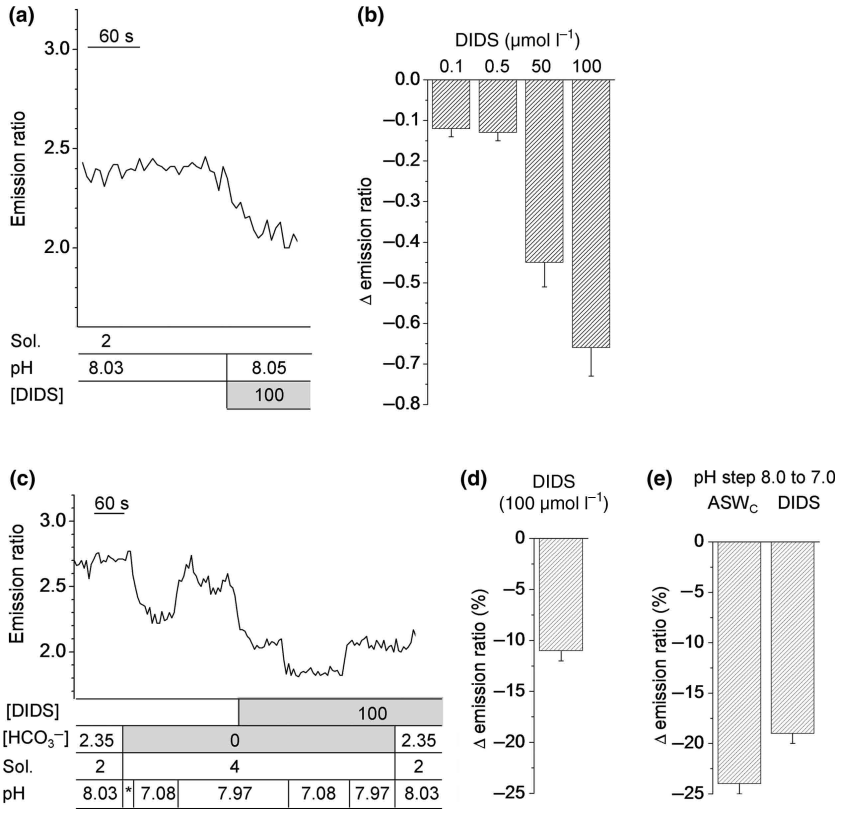

Fig. 6 Effect of 4,4′-diisothiocyanatostilbene-2,2′-disulfonic acid (DIDS) on intracellular pH (pH_i). (a) Original recording of fluorescence ratio as a measure of pH_i in a single cell of *Emiliania huxleyi*. Effect of DIDS (100 μmol l^{-1}) in the presence of HCO_3^-. (b) Concentration response for the effect of DIDS on pH_i in the presence of HCO_3^- given as absolute change in fluorescence ratio (Δ) (m = 2, n = 11). (c) Original recording of fluorescence ratio as a measure of pH_i in a single cell. Effect of DIDS (100 μmol l^{-1}) in the absence of HCO_3^-. Comparison of the effect of seawater pH (pH_e) of 7 on pH_i in the absence and presence of DIDS. (d) Relative change in fluorescence ratio by DIDS in the absence of HCO_3^- (m = 3, n = 46). (e) Relative change in fluorescence ratio by pH_e 7 in the absence and presence of DIDS (m = 3, n = 46). Relative changes in ratio differed significantly (P < 0.01). ASW_c, control artificial seawater (solution (Sol.) 2); Sol. 4, 0 HCO_3^- solution.

decipher the subcellular processes involved in acid–base metabolism.

To identify the individual effects of [CO_2], [HCO_3^-] and [H^+] on the cell's acid–base metabolism, we generated experimental conditions which enabled us to test for changes in pH_i in response to separate, single-parameter changes of H^+, CO_2 and HCO_3^- in the external medium (Zhao *et al.*, 1995, 2003). Calculations confirmed that the time-frame of the experiments was well within the time-frame of disequilibrium of the carbonate system.

Dye loading and intracellular pH

2′,7′-Bis-(2-carboxyethyl)-5-(and-6)-carboxyfluorescein measurements of pH_i in *E. huxleyi* have already been established (Dixon *et al.*, 1989) and values for overall pH_i were recorded in the range of 7.1–7.3 in the presence of 2 mmol l^{-1} HCO_3^-. In line with Anning *et al.* (1996), our observations confirm the unequal dye loading intensity between cells within the same batch. This has been attributed to different stages of the cell cycle and the respective expression of esterase activity. In addition, we observed a larger scatter of resting fluorescence ratios (Fig. 2) for the individual cells of the same batch, which was independent of dye loading. This could be caused by real differences in pH_i values between cells and thus by their individual functional state. However, since the relationship between pH_i and fluorescence ratio depends on the intracellular composition, it could also originate from different individual BCECF calibration curves for each cell. In favor of an optimal time window for the experiment with respect to fluorescence intensity and cell viability, we decided not to perform an individual calibration for each cell and focussed on relative changes of pH_i.

However, we carried out calibration experiments in a separate experimental series to obtain the values of pH_i change corresponding to the respective changes in fluorescence ratio. Although we describe a substantial H^+ permeability in *E. huxleyi*, the calibration experiments show that the respective pathway is still limiting and that pH_i does not decrease as rapidly, or to as great an extent, as after permeabilization by nigericin (Fig. 4b). The respective slopes of pH_i response

show that *E. huxleyi* follow pH_e changes by *c.* 56%. This means that a pH_e change of 1 is needed to acidify the cell by 0.56 pH units. This difference suggests the presence of mechanisms which counteract cellular acidification, for example by H^+ metabolism. This is also supported by the rapid kinetics of realkalinization on return to control conditions in Fig. 4(b).

It remains open how close our cells were to the reported absolute pH_i values when entering the experiments. In fact, they could be different since the previous studies with *E. huxleyi* were performed in a minimal medium consisting of 30 mmol l^{-1} NaCl, HEPES buffer, 2 mmol l^{-1} HCO_3^- and mannitol (Dixon *et al.*, 1989). Properties of our experimental control solutions were adjusted to mimic natural seawater. The main differences were the presence of $[Na^+]$ and $[Cl^-]$ close to natural concentrations. This might significantly influence pH_i and the capability of the cells to maintain pH homeostasis, as it is likely that Na^+- and Cl^--dependent mechanisms are involved in H^+ and HCO_3^- transport. In addition, membrane voltage in coccolithophores strongly depends on either K^+ or Cl^- conductance (Sikes & Wilbur, 1982; Taylor & Brownlee, 2003) and the respective electrochemical driving forces (i.e. ion gradients).

We did not observe a dye signal from the chloroplast (cf. confocal image, Fig. 2b). The detected fluorescence signal thus resembles an integrated signal of the whole cell with a major contribution by the cytosol. However, we cannot exclude a partial contribution of compartmentalized dye to the integrated signal.

In some cases we observed a slight decrease in the ratio over time. At present we have no clear explanation for this. It may reflect an acidification of the cells over the time course of the experiment or a change in the contribution of compartmentalized dye to the integrated signal.

Membrane H^+ permeability

We observed a dramatic and instant change in pH_i with a change in the pH_e. The kinetics of this effect was fast, on the order of the bath exchange rate, which was 6–8 ml min^{-1} at a bath volume of 350 µl, corresponding to an exchange time constant of *c.* 2.4 s. This indicates that the effect of acidified pH_e was most likely directly via the influx of acid equivalents or the impairment of efflux of continuously produced H^+. Any indirect effects using more complex intracellular metabolic events would have been expected on a slower timescale.

The plasma membrane properties do not normally allow any passive H^+ flux. Diffusion of protons across biological membranes can be facilitated by a number of specialized proteins which could support the observed effect: facilitated CO_2 influx via aquaporins and subsequent formation and dissociation of carbonic acid in the presence of CA; carrier proteins which use the transmembrane gradient for one substrate (e.g. Cl^-) for the transport of another substrate (e.g. HCO_3^-) against its concentration gradient; ion channels providing a conductive permeability (e.g. H^+).

To distinguish among these possibilities we generated experimental solutions which allowed the isolated change of CO_2 and HCO_3^- or of H^+ in the absence of DIC. Our results clearly show that a conductive or carrier-mediated H^+ pathway underlies the high proton permeability of the membrane. Since we did not observe any saturation or nonlinear behavior within the investigated pH range, a proton conductance via H^+ channels is the most likely candidate.

We did not observe a pH_i recovery under the continuous exposure to acidified pH_e. After return to control conditions the cells again followed pH_e passively and did not show any sign of overcompensation. Some cells, however, remained slightly more acidic after the experiment.

On first sight this would suggest a cell with low pH regulatory capacity or even low metabolism. On the other hand, since calcifying *E. huxleyi* produce large amounts of H^+ (Dong *et al.*, 1993; Anning *et al.*, 1996), as long as photosynthesis and calcification are not synchronized, the existence of a significant H^+ export pathway could support the maintenance of pH homeostasis. This pathway would then mask regulatory mechanisms with lower transport capacity. Assuming a conductive H^+ pathway, membrane voltage in *E. huxleyi* would gain a predominant role in pH_i homeostasis and become decisive for the export of H^+ and hence for the ability to calcify. However, it remains open if these properties are limited to the functional state of *E. huxleyi* in this study (nutrient limitation and high calcification) or if we observed a general property.

High CO_2 (pH 8.08, *c.* 600 µmol kg^{-1} CO_2, 250 µmol kg^{-1} HCO_3^-)

The cells were exposed to (continuously freshly supplied) OOE solution for a considerable time span. By this procedure the carbonate system in the solution outside the cell was not allowed to equilibrate. At the same time, however, the intracellular compartment can react on the respective $[CO_2]$. Membrane permeability for CO_2, metabolism and buffering then determine the effect on pH_i.

In our hands the isolated increase in CO_2 did not cause any detectable change in pH_i. This was surprising since a considerable CO_2 permeability and thus CO_2 leakage of the *E. huxleyi* cell membrane has been postulated (Rost *et al.*, 2006) and a consecutive acidification of the cytosol would then be expected after intracellular formation and dissociation of carbonic acid. This should occur even if baseline intracellular $[CO_2]$ would be high as a result of overcalcification. Most cell membranes show intrinsic CO_2 permeability and, in addition, there are membrane proteins like aquaporins (Musa-Aziz *et al.*, 2009) which facilitate CO_2 diffusion. In fact, the *E. huxleyi* genome reveals several candidate aquaporins which might be func-

tionally relevant (von Dassow *et al.*, 2009 and references therein).

On the other hand, there are examples of membranes with very limited CO_2 permeability, such as in kidney and gastrointestinal tract luminal epithelia (Bleich *et al.*, 1995; Hasselblatt *et al.*, 2000). In any case, acidification by an extracellular [CO_2] increase would only be visible at a significant activity of CA and at limited membrane permeability for H^+. In fact, in our experiments, we show high H^+ permeability. Even if CO_2 permeability is also high, and intracellular CAs (Soto *et al.*, 2006) are very active, the rates of H^+ production would be overwhelmed by the high proton permeability, masking intracellular generation of H^+ as a result of conversion of CO_2. Finally, CO_2 could be trapped immediately by photosynthesis, bypassing metabolic conversion within the cytosol. However, our experimental conditions render this alternative unlikely: illumination times in the experimental setup were kept very short (24 and 60 ms on 486 and 440 nm, respectively), and illumination only took place every 5 s. These conditions should not drive photosynthesis significantly; even if photosynthesis was activated by the conditions, at 600 μmol kg^{-1} CO_2 Rubisco is well saturated even at highest light, assuming the low CO_2 affinity in *E. huxleyi* as found by Shiraiwa *et al.* (2004).

Against this background and given our observations on H^+ permeability, it is not surprising that an isolated change in [CO_2] did not affect pH_i. However, we are not able to give an estimate of the plasma membrane CO_2 permeability at this stage. Further experiments to clarify this question would require inhibitors of the H^+ pathway, of photosynthesis and a reassessment of CA activity.

High HCO_3^- (pH 8.07, *c.* 50 μmol kg^{-1} CO_2, 19.7 mmol kg^{-1} HCO_3^-)

The isolated increase in extracellular [HCO_3^-] led to a decrease in pH_i. This was surprising since one would expect rather an alkalinization at a cellular pH_i of *c.* 7.2 since uptake of HCO_3^- and subsequent cytosolic H^+ buffering would increase pH_i. The observed decrease in pH_i might be caused by immediate metabolism of HCO_3^- to CO_3^{2-} and H^+ (Anning *et al.*, 1996). *E. huxleyi* continuously requires high amounts of CO_3^{2-} for coccolith formation and the respective metabolism of HCO_3^- would generate H^+ and decrease pH_i, irrespective of whether CO_3^{2-} formation occurs within the cytosol or inside the coccolith vesicle. An alternative would be cotransport of HCO_3^- with H^+ or antiport of HCO_3^- vs OH^- or Cl^-. If any of these transporters were electrogenic the increased exchange could result in a change in membrane voltage which would directly influence the proton current through putative proton channels.

However, why is the respective H^+ load by metabolism or cotransport not short-circuited by the observed H^+ permeability? In contrast to the experiment with an isolated increase in [CO_2], providing 0.6 mmol kg^{-1} CO_2, the isolated increase in [HCO_3^-] provides 19.7 mmol kg^{-1} HCO_3^- at the experimental time slot, resulting in a 33-fold higher substrate concentration for the respective generation of H^+. Under these conditions the H^+ pathway might become limiting.

DIDS effect

4,4′-Diisothiocyanatostilbene-2,2′-disulfonic acid has been used as a blocker of a variety of transporters involved in pH homeostasis and HCO_3^- transport (Romero *et al.*, 2004). In contrast to Nimer *et al.* (1996) who did not find a DIDS-sensitive HCO_3^- transport in exponentially growing *E. huxleyi* cells, Herfort *et al.* (2002) found a DIDS- and SITS-inhibitable HCO_3^--sensitive system and postulated an anion exchanger (AE1). In our experiments DIDS caused a decrease in pH_i which was not dependent on external HCO_3^-. As the effect of acidified pH_e on pH_i was decreased in the presence of DIDS, it might interfere directly with the H^+ permeability in *E. huxleyi*. On the other hand, it might also be a less specific effect on the H^+ current, for example by affecting the Cl^- conductance and the membrane potential. In fact, in *C. pelagicus*, DIDS sensitivity of an inward Cl^- rectifier channel has been shown (Taylor & Brownlee, 2003). This channel might be involved in balancing H^+ and HCO_3^- directly or indirectly via membrane voltage regulation.

At this stage it is completely open which membrane protein provides the H^+ pathway, how it is regulated, and what other transport systems it might be dependent on. At least for the ClC family of Cl^- coupled H^+ transporters, DIDS inhibition has been reported (Pusch *et al.*, 2006). This could be a starting point for the search of candidate proteins involved in *E. huxleyi* membrane H^+ transport.

Synthesis

Taken together, we show for the first time a proton permeability in *E. huxleyi*. The decrease of pH_i as a result of increased extracellular [HCO_3^-] suggests a predominant metabolism of HCO_3^- to H^+ and CO_3^{2-}. Considering the effect of DIDS on pH_i, DIDS may serve as a useful tool to further examine the properties of H^+ transport in *E. huxleyi*. The data reveal that pH_i in *E. huxleyi* is directly affected by seawater pH. The underlying membrane proteins are candidates for the investigation of long-term adaptation potential of *E. huxleyi* to ocean acidification.

Acknowledgements

Marius N. Müller is acknowledged for providing *E. huxleyi*. We are grateful to the workshop of the Physiological

Institute, especially Holger Voigt, for construction of special technical equipment. We kindly acknowledge technical assistance by Thomas Stegmann and Regina Lingg. The project has been performed and supported within the cluster of excellence 'The Future Ocean', CP0602 and CP0701, at the Christian-Albrechts-Universität zu Kiel. We thankfully acknowledge the support of Federal Ministry of Education and Research (BMBF; FKZ 03F0608M).

References

Anning T, Nimer NA, Merrett MJ, Brownlee C. 1996. Costs and benefits of calcification in coccolithophorids. *Journal of Marine Systems* **9**: 45–56.

Balch WM, Holligan PM, Ackleson SG, Voss KJ. 2010. Biological and optical properties of mesoscale coccolithophore blooms in the Gulf of Maine. *Limnology and Oceanography* **36**: 629–643.

Bleich M, Köttgen M, Schlatter E, Greger R. 1995. Effect of NH_4^+/NH_3 on cytosolic pH and the K^+ channels of freshly isolated cells from the thick ascending limb of Henle's Loop. *Pflügers Archiv – European Journal of Physiology* **429**: 345–354.

Broecker W, Clark E. 2009. Ratio of coccolith $CaCO_3$ to foraminifera $CaCO_3$ in late Holocene deep sea sediments. *Paleoceanography* **24**: 11.

Brownlee C, Taylor AR. 2004. Calcification in coccolithophores: a cellular perspective. In: Thierstein HR, Young JR, eds. *Coccolithophores-from molecular processes to global impact*. Berlin, Germany: Springer, 31–49.

von Dassow P, Ogata H, Probert I, Wincker P, Da Silva C, Audic S, Claverie JM, de Vargas C. 2009. Transcriptome analysis of functional differentiation between haploid and diploid cells of *Emiliania huxleyi*, a globally significant photosynthetic calcifying cell. *Genome Biology* **10**: 33.

Dickson AG. 1990. Standard potential of the reaction – AgCl(S)+1/2H-2(G)=Ag(S)+HCl(Aq) and the standard acidity constant of the ion HSO_4^- in synthetic sea-water from 273.15-K to 318.15-K. *Journal of Chemical Thermodynamics* **22**: 113–127.

Dixon GK, Brownlee C, Merrett MJ. 1989. Measurement of internal pH in the coccolithophore *Emiliania huxleyi* using 2′,7′-bis-(2-carboxyethyl)-5(and-6)carboxyfluorescein acetoxymethylester and digital imaging microscopy. *Planta* **178**: 443–449.

Dong LF, Nimer NA, Okus E, Merrett MJ. 1993. Dissolved inorganic carbon utilization in relation to calcite production in *Emiliania huxleyi* (Lohmann) Kamptner. *New Phytologist* **123**: 679–684.

Endeward V, Musa-Aziz R, Cooper GJ, Chen LM, Pelletier MF, Virkki LV, Supuran CT, King LS, Boron WF, Gros G. 2006. Evidence that aquaporin 1 is a major pathway for CO_2 transport across the human erythrocyte membrane. *FASEB Journal* **20**: 1974–1981.

Guillard RRL. 1975. Culture of phytoplankton for feeding marine invertebrates. In: Smith WL, Chanley MH, eds. *Culture of marine invertebrate snimals*. New York, NY, USA: Plenum Press, 26–60.

Hasselblatt P, Warth R, Schulz-Baldes A, Greger R, Bleich M. 2000. pH regulation in isolated *in vitro* perfused rat colonic crypts. *Pflügers Archiv – European Journal of Physiology* **441**: 118–124.

Herfort L, Thake B, Roberts J. 2002. Acquisition and use of bicarbonate by *Emiliania huxleyi*. *New Phytologist* **156**: 427–436.

Ho T-Y, Quigg A, Finkel ZV, Milligan AJ, Wyman K, Falkowski PG, Morel FMM. 2003. The elemental composition of some marine phytoplankton. *Journal of Phycology* **39**: 1–15.

Holligan PM, Viollier M, Harbour DS, Camus P, Champagnephilippe M. 1983. Satellite and ship studies of coccolithophore production along a continental-shelf edge. *Nature* **304**: 339–342.

Kester D, Duedall I, Connors D, Pytkowicz R. 1967. Preparation of artificial seawater. *Limnology and Oceanography* **12**: 176–179.

Lewis E, Wallace DWR. 1998. CO2SYS_Calc_DOS_Original: program developed for CO_2 system calculations. *ORNL/CDIAC-105*. Oak Ridge, Tennessee: Carbon Dioxide Information Analysis Center, Oak Ridge National Laboratory, US Department of Energy.

Musa-Aziz R, Chen LM, Pelletier MF, Boron WF. 2009. Relative CO_2/NH_3 selectivities of AQP1, AQP4, AQP5, AmtB, and RhAG. *Proceedings of the National Academy of Sciences, USA* **106**: 5406–5411.

Nimer NA, Brownlee C, Merrett MJ. 1994a. Carbon dioxide availability, intracellular pH and growth rate of the coccolithophore *Emiliania huxleyi*. *Marine Ecology-Progress Series* **109**: 257–262.

Nimer NA, Guan Q, Merrett MJ. 1994b. Extracellular and intracellular carbonic-Anhydrase in relation to culture age in a high-calcifying strain of *Emiliania huxleyi* Lohmann. *New Phytologist* **126**: 601–607.

Nimer NA, Merrett MJ, Brownlee C. 1996. Inorganic carbon transport in relation to culture age and inorganic carbon concentration in a high-calcifying strain of *Emiliania huxleyi* (Prymnesiophyceae). *Journal of Phycology* **32**: 813–818.

Paasche E. 1968. Effect of temperature light intensity and photoperiod on voccolith formation. *Limnology and Oceanography* **13**: 178.

Paasche E. 2002. A review of the coccolithophorid *Emiliania huxleyi* (Prymnesiophyceae), with particular reference to growth, coccolith formation, and calcification–photosynthesis Interactions. *Phycologia* **40**: 503–529.

Pörtner H-O, Bickmeyer U, Bleich M, Bock C, Brownlee C, Melzner F, Michaelidis B, Sartoris FJ, Storch D 2010. Part 3, measurements of CO_2-sensitive processes. Chapter 9: studies of acid–base status and regulation. In: Riebesell U, Fabry VJ, Hansson L, Gattuso J-P, eds. *Guide to best practices for ocean acidification research and data reporting*. Luxembourg City, Luxembourg: Publications Office of the European Union.

Pressman BC. 1976. Biological applications of ionophores. *Annual Review of Biochemistry* **45**: 501–530.

Pusch M, Zifarelli G, Murgia AR, Picollo A, Babini E. 2006. Channel or transporter? The CLC saga vontinues. *Experimental Physiology* **91**: 149–152.

Riebesell U, Schulz KG, Bellerby RGJ, Botros M, Fritsche P, Meyerhofer M, Neill C, Nondal G, Oschlies A, Wohlers J *et al.* 2007. Enhanced biological carbon consumption in a high CO_2 ocean. *Nature* **450**: 545–548.

Rink TJ, Tsien RY, Pozzan T. 1982. Cytoplasmic pH and free Mg^{2+} in lymphocytes. *Journal of Cell Biology* **95**: 189–196.

Romero MF, Fulton CM, Boron WF. 2004. The SLC4 family of HCO_3^- transporters. *Pflügers Archiv – European Journal of Physiology* **447**: 495–509.

Rost B, Riebesell U, Burkhardt S, Sultemeyer D. 2003. Carbon acquisition of bloom-forming marinephytoplankton. *Limnology and Oceanography* **48**: 55–67.

Rost B, Riebesell U, Sultemeyer D. 2006. Carbons acquisition of marine phytoplankton: effect of photoperiod length. *Limnology and Oceanography* **51**: 12–20.

Rost B, Zondervan I, Riebesell U. 2002. Light-dependent carbon isotope fractionation in the coccolithophorid *Emiliania huxleyi*. *Limnology and Oceanography* **47**: 120–128.

Roy RN, Roy LN, Vogel KM, Porter-Moore C, Pearson T, Good CE, Millero FJ, Campbell DM. 1993. The dissociation constants of carbonic acid in seawater at salinities 5 to 45 and temperatures 0 to 45°C. *Marine Chemistry* **44**: 249–267.

Schulz KG, Riebesell U, Rost B, Thoms S, Zeebe RE. 2006. Determination of the rate constants for the carbon dioxide to bicarbonate inter-conversion in pH-buffered seawater systems. *Marine Chemistry* **100**: 53–65.

Shampine LF, Reichelt MW. 1997. The Matlab Ode Suite. *Siam Journal on Scientific Computing* **18**: 1–22.

Shiraiwa Y. 2003. Physiological regulation of carbon fixation in the photosynthesis and calcification of coccolithophorids. *Comparative Biochemistry and Physiology Part B* **136**: 775–783.

Shiraiwa Y, Danbara A, Yoke K. 2004. Characterization of highly oxygen-sensitive photosynthesis in coccolithophorids. *Japanese Journal of Phycology* **52**: 87–94.

Sikes CS, Wilbur KM. 1982. Functions of coccolith formation. *Limnology and Oceanography* **27**: 18–26.

Soto AR, Zheng H, Shoemaker D, Rodriguez J, Read BA, Wahlund TM. 2006. Identification and preliminary characterization of two CDNAs encoding unique carbonic anhydrases from the marine alga *Emiliania huxleyi*. *Applied and Environmental Microbiology* **72**: 5500–5511.

Taylor AR, Brownlee C. 2003. A Novel Cl^- inward-rectifying current in the plasma membrane of the calcifying marine phytoplankton *Coccolithus pelagicus*. *Plant Physiology* **131**: 1391–1400.

Tsuji Y, Suzuki I, Shiraiwa Y. 2009. Photosynthetic carbon assimilation in the coccolithophorid *Emiliania huxleyi* (Haptophyta): evidence for the predominant operation of the C-3 cycle and the contribution of β-carboxylases to the active anaplerotic reaction. *Plant and Cell Physiology* **50**: 318–329.

Westbroek P, Brown CW, Vanbleijswijk J, Brownlee C, Brummer GJ, Conte M, Egge J, Fernandez E, Jordan R, Knappertsbusch M *et al.* 1993. A model system approach to biological climate forcing – the example of *Emiliania huxleyi*. *Global and Planetary Change* **8**: 27–46.

Westbroek P, Young JR, Linschooten K. 1989. Coccolith production (biomineralization) in the marine alga *Emiliania huxleyi*. *Journal of Protozoology* **36**: 368–373.

Zeebe RE, Wolf-Gladrow DA. 2001. CO_2 in seawater: equilibrium, kinetics, isotopes. In: Halpern D, ed. *Elsevier oceanography series*, Vol 65. Amsterdam, the Netherlands: Elsevier, 346.

Zhao J, Zhou Y, Boron WF. 2003. Effect of isolated removal of either basolateral HCO_3^- or basolateral CO_2 on HCO_3^- reabsorption by rabbit S2 proximal tubule. *American Journal of Physiology – Renal Physiology* **285**: F359–F369.

Zhao JH, Hogan EM, Bevensee MO, Boron WF. 1995. Out-of-equilibrium CO_2/HCO_3^- solutions and their use in characterizing a new K/HCO_3 cotransporter. *Nature* **374**: 636–639.

Supporting Information

Additional supporting information may be found in the online version of this article.

Fig. S1 Out-of-equilibrium (OOE) mixing unit and bath chamber.

Please note: Wiley-Blackwell are not responsible for the content or functionality of any supporting information supplied by the authors. Any queries (other than missing material) should be directed to the *New Phytologist* Central Office.